nature physics

SUPPLEMENTARY INFORMATION
https://doi.org/10.1038/s41567-018-0310-x

In the format provided by the authors and unedited.

Spin pumping from nuclear spin waves

Yuki Shiomi[1,5,6,7*], Jana Lustikova[1,7], Shingo Watanabe[1], Daichi Hirobe[1], Saburo Takahashi[1,2] and Eiji Saitoh[1,2,3,4*]

[1]Institute for Materials Research, Tohoku University, Sendai, Japan. [2]Center for Spintronics Research Network, Tohoku University, Sendai, Japan. [3]Advanced Science Research Center, Japan Atomic Energy Agency, Tokai, Japan. [4]Advanced Institute for Materials Research, Tohoku University, Sendai, Japan. [5]RIKEN Center for Emergent Matter Science (CEMS), Wako, Japan. [6]Present Address: Department of Applied Physics and Quantum-Phase Electronics Center (QPEC), University of Tokyo, Tokyo, Japan. [7]These authors contributed equally: Yuki Shiomi and Jana Lustikova. *e-mail: shiomi@ap.t.u-tokyo.ac.jp; eizi@ap.t.u-tokyo.ac.jp

Supplementary Information for

"Spin pumping from nuclear spin waves"

Table of Contents:

(a) Theoretical calculation for nuclear spin pumping

The coupled equations of electron sublattice magnetization vectors $\mathbf{M}_1$ and $\mathbf{M}_2$ and the corresponding nuclear magnetization vectors $\mathbf{m}_1$ and $\mathbf{m}_2$ in the two sublattices of an antiferromagnet $MnCO_3$ are [S1,S2]

$$\frac{\partial}{\partial t}\mathbf{M}_1 = -\gamma_e \mathbf{M}_1 \times \left[\mathbf{H} + \mathbf{h} + \mathbf{H}_\mathrm{A} - KM_{1y}\mathbf{e}_y - \lambda_M \mathbf{M}_2 - D(\mathbf{M}_2 \times \mathbf{e}_y) + \lambda_m \mathbf{m}_1\right] + \alpha_0\left(\frac{\mathbf{M}_1}{M_0} \times \frac{\partial}{\partial t}\mathbf{M}_1\right) + \boldsymbol{\tau}_1^{\mathrm{STT}},$$

$$\frac{\partial}{\partial t}\mathbf{M}_2 = -\gamma_e \mathbf{M}_2 \times \left[\mathbf{H} + \mathbf{h} - \mathbf{H}_\mathrm{A} - KM_{2y}\mathbf{e}_y - \lambda_M \mathbf{M}_1 + D(\mathbf{M}_1 \times \mathbf{e}_y) + \lambda_m \mathbf{m}_2\right] + \alpha_0\left(\frac{\mathbf{M}_2}{M_0} \times \frac{\partial}{\partial t}\mathbf{M}_2\right) + \tau_2^{\mathrm{STT}},$$

$$\frac{\partial}{\partial t}\mathbf{m}_1 = \gamma_n \mathbf{m}_1 \times (\mathbf{H} + \mathbf{h} + \lambda_m \mathbf{M}_1) - \frac{\mathbf{m}_1^{\parallel} - \mathbf{m}_{10}}{T_1} - \frac{\mathbf{m}_1^{\perp}}{T_2},$$

$$\frac{\partial}{\partial t}\mathbf{m}_2 = \gamma_n \mathbf{m}_2 \times (\mathbf{H} + \mathbf{h} + \lambda_m \mathbf{M}_2) - \frac{\mathbf{m}_2^{\parallel} - \mathbf{m}_{20}}{T_1} - \frac{\mathbf{m}_2^{\perp}}{T_2}.$$

Here, γ_e and γ_n are the gyromagnetic ratios for electron and nuclear spins, respectively, $\mathbf{H}_\mathrm{A} = (H_\mathrm{A}, 0, 0)$ is an anisotropy magnetic field in the {111} plane (x-z plane), K is a parameter of out-of-plane magnetic anisotropy, λ_M and λ_m are the dimensionless spin exchange parameters for the M_1-M_2 coupling and the electron-nuclear spin coupling, respectively, D is a Dzyaloshinskii-Moriya parameter, α_0 is an intrinsic Gilbert damping constant, $\boldsymbol{h} = (h_x, 0, 0)$ is an rf magnetic field, T_1 and T_2 are longitudinal and transverse spin-spin relaxation times, $\mathbf{m}_{1(2)}^{\parallel}$ and $\mathbf{m}_{1(2)}^{\perp}$ are the parallel and perpendicular components of $\mathbf{m}_{1(2)}$ with respect to the equilibrium $\mathbf{m}_{10(20)}$, $\mathbf{e}_y$ is the unit vector in the y direction parallel to the antiferromagnetic axis, and $M_0 = |\mathbf{M}_1| = |\mathbf{M}_2|$ is the magnitude of the sublattice magnetization.

Spin transfer torque $\boldsymbol{\tau}_1^{\mathrm{STT}}$ and $\boldsymbol{\tau}_2^{\mathrm{STT}}$ related to spin pumping as well as absorption of a transverse spin current are derived based on a spin diffusion model with the quantum mechanical boundary conditions [S3,S4] in a Pt/$MnCO_3$ bilayer

$$\boldsymbol{\tau}_1^{\mathrm{STT}} = \alpha_{\mathrm{SP}}^0 \hbar\left(\frac{\mathbf{M}_1}{M_0} \times \frac{\partial \mathbf{M}_1}{\partial t}\right) - \alpha_{\mathrm{BF}}^0 \hbar\left(\frac{\mathbf{M}_1}{M_0} \times \frac{\partial \mathbf{M}_1}{\partial t} + \frac{\mathbf{M}_2}{M_0} \times \frac{\partial \mathbf{M}_2}{\partial t}\right),$$

$$\boldsymbol{\tau}_2^{\mathrm{STT}} = \alpha_{\mathrm{SP}}^0 \hbar\left(\frac{\mathbf{M}_2}{M_0} \times \frac{\partial \mathbf{M}_2}{\partial t}\right) - \alpha_{\mathrm{BF}}^0 \hbar\left(\frac{\mathbf{M}_1}{M_0} \times \frac{\partial \mathbf{M}_1}{\partial t} + \frac{\mathbf{M}_2}{M_0} \times \frac{\partial \mathbf{M}_2}{\partial t}\right).$$

Here, α_{SP}^{0} and α_{BF}^{0} are the effective Gilbert damping constants for spin pumping and absorption of a backflow spin current, respectively, given by

$$\alpha_{\mathrm{SP}}^{0}=\frac{\hbar}{2e^{2}}\frac{\gamma}{M_{0}d_{\mathrm{F}}}G_{\uparrow\downarrow},$$

$$\alpha_{\mathrm{BF}}^{0}=\alpha_{\mathrm{SP}}^{0}\frac{2\rho_{\mathrm{N}}\lambda_{\mathrm{N}}G_{\uparrow\downarrow}\coth(d_{\mathrm{N}}/\lambda_{\mathrm{N}})}{1+4\rho_{\mathrm{N}}\lambda_{\mathrm{N}}G_{\uparrow\downarrow}\coth(d_{\mathrm{N}}/\lambda_{\mathrm{N}})},$$

where $G_{\uparrow\downarrow}$ is the interface spin-mixing conductance and ρ_{N} and λ_{N} are the resistivity and the spin-diffusion length of the Pt layer, respectively.

Rewriting the coupled equation in terms of $\mathbf{M}=(\mathbf{M}_1+\mathbf{M}_2)/2$, $\mathbf{N}=(\mathbf{M}_1-\mathbf{M}_2)/2$, $\mathbf{m}=(\mathbf{m}_1+\mathbf{m}_2)/2$, and $\mathbf{n}=(\mathbf{n}_1-\mathbf{n}_2)/2$, we have

$$\begin{aligned}\frac{\partial}{\partial t}\mathbf{M}=&-\gamma_e\mathbf{M}\times\mathbf{H}-\gamma_e\mathbf{M}\times\mathbf{h}-\gamma_e H_{\mathrm{A}}\mathbf{N}\times\mathbf{e}_x+\gamma_e K\left(M_y\mathbf{M}+N_y\mathbf{N}\right)\times\mathbf{e}_y+D\left(M_x\mathbf{N}-N_x\mathbf{M}\right)\times\mathbf{e}_z\\&-D\left(M_z\mathbf{N}-N_z\mathbf{M}\right)\times\mathbf{e}_x-\gamma_e\lambda_m\left[\mathbf{M}\times\mathbf{m}+\mathbf{N}\times\mathbf{n}\right]+\frac{\alpha_M}{M_0}\hbar\left(\mathbf{M}\times\frac{\partial\mathbf{M}}{\partial t}+\mathbf{N}\times\frac{\partial\mathbf{N}}{\partial t}\right),\end{aligned}$$

$$\begin{aligned}\frac{\partial}{\partial t}\mathbf{N}=&-\gamma_e\mathbf{N}\times\mathbf{H}-\gamma_e\mathbf{N}\times\mathbf{h}-\gamma_e H_{\mathrm{A}}\mathbf{M}\times\mathbf{e}_x+\gamma_e K\left(N_y\mathbf{M}+M_y\mathbf{N}\right)\times\mathbf{e}_y+D\left(M_x\mathbf{M}-N_x\mathbf{N}\right)\times\mathbf{e}_z\\&-D\left(M_z\mathbf{M}-N_z\mathbf{N}\right)\times\mathbf{e}_x-\gamma_e\lambda_m\left[\mathbf{M}\times\mathbf{n}+\mathbf{N}\times\mathbf{m}\right]-2\lambda_M\gamma_e\left(\mathbf{M}\times\mathbf{N}\right)\\&+\frac{\alpha_N}{M_0}\hbar\left(\mathbf{M}\times\frac{\partial\mathbf{N}}{\partial t}+\mathbf{N}\times\frac{\partial\mathbf{M}}{\partial t}\right),\end{aligned}$$

$$\frac{\partial}{\partial t}\mathbf{m}=\gamma_n\mathbf{m}\times\mathbf{H}+\gamma_n\mathbf{m}\times\mathbf{h}+\gamma_n\left(\lambda_m\mathbf{m}\times\mathbf{M}+\lambda_m\mathbf{n}\times\mathbf{N}\right)-\frac{\mathbf{m}^{\parallel}-\mathbf{m}_0}{T_1}-\frac{\mathbf{m}^{\perp}}{T_2},$$

$$\frac{\partial}{\partial t}\mathbf{n}=\gamma_n\mathbf{n}\times\mathbf{H}+\gamma_n\mathbf{n}\times\mathbf{h}+\gamma_n\left(\lambda_m\mathbf{n}\times\mathbf{M}+\lambda_m\mathbf{m}\times\mathbf{N}\right)-\frac{\mathbf{n}^{\parallel}-\mathbf{n}_0}{T_1}-\frac{\mathbf{n}^{\perp}}{T_2},$$

where $\alpha_M=\alpha_0+\alpha_{\mathrm{SP}}^{0}/\left[1+4\rho_{\mathrm{N}}\lambda_{\mathrm{N}}G_{\uparrow\downarrow}\coth(d_{\mathrm{N}}/\lambda_{\mathrm{N}})\right]$ and $\alpha_N=\alpha_0+\alpha_{\mathrm{SP}}^{0}$. By solving the coupled equations, we obtain the secular equation for δM_y and δm_y and find the NMR frequency [S1,S2,S5-S6]

$$\omega=\gamma_n H_p^{*}\approx\gamma_n H_n\sqrt{1-\frac{H_a H_s}{H\left(H+H_{\mathrm{D}}\right)+\left(H_{\mathrm{A}}+H_a\right)H_s}}.$$

Here, we assumed that the in-plane and out-of-plane anisotropic magnetic fields, H_{A} (~1Oe) and $H_{\mathrm{K}}=KM_0$ (~2 kOe), are much less than the effective magnetic field originating from the spin exchange coupling $H_s = 6.8 \times 10^5$ Oe [S1,S2]. $H_n = \lambda_m M_0 = A\langle S\rangle/\hbar\gamma_n$ (~574 kOe) [S1,S2] is an average hyperfine field acting on the nucleus, $H_D = DM_0 = 4.4 \times 10^3$ Oe [S7] is the magnetic field originating from the Dzyaloshinskii-Moriya interaction which gives rise to a small canted angle of the order of $\theta \approx (H_D/H_s) \ll 1$, and H_a is the additional anisotropic magnetic field originating from the hyperfine interaction: $H_a = \lambda_m m_0 = A\langle I\rangle/\hbar\gamma_e$, which is a control parameter for the fitting to the experimental results in Fig. 2**b**. As shown in the main text, $(\gamma_n H_n/2\pi)$ is 640 MHz. The nuclear spin polarization can be estimated by the relation $\langle I\rangle = S(\gamma_e/\gamma_n)(H_a/H_n)$. Using the data of H_a in Fig. 2**b**, $\langle I\rangle/I \sim 0.8\%$ at 3.5K and $\langle I\rangle/I \sim 2.3\%$ at 1.5K.

The NMR linewidth Δ due to the spin pumping, which is plotted in Fig. 4**d**, is

$$\Delta = \Delta_0\left[1-(H_p^*/H_n)^2\right]^2 + T_2^{-1},$$

where $\Delta_0 = \alpha_M(\gamma_n H_n)^2/(2\gamma_e H_a)$. In the calculation shown in Fig. 4**d**, we used the values of $1/(T_2\Delta_0) = 0.005$, $\Delta_0 = 1.0\times10^8\ \mathrm{s}^{-1}$, and $H_a = 5.5$ Oe at 1.5 K.

The inverse spin Hall voltage induced by nuclear spin pumping is given by

$$\begin{aligned} V &= 2e\theta_{\mathrm{SH}}\rho_{\mathrm{N}}L_V\frac{\lambda_{\mathrm{N}}}{d_{\mathrm{N}}}\tanh(d_{\mathrm{N}}/2\lambda_{\mathrm{N}})\frac{M_s d_{\mathrm{F}}}{\hbar\gamma}\left(\boldsymbol{\tau}_1^{\mathrm{STT}}+\boldsymbol{\tau}_2^{\mathrm{STT}}\right) \\ &= \theta_{\mathrm{SH}}\frac{\hbar}{2e}\frac{L_V}{d_{\mathrm{N}}}g_m M_0^{-2}\left[\boldsymbol{M}\times(\partial\boldsymbol{M}/\partial t)\right]_z, \end{aligned}$$

where L_V is the distance between the electrodes for the voltage measurement and

$$g_m = \frac{4\rho_{\mathrm{N}}\lambda_{\mathrm{N}}G_{\uparrow\downarrow}\tanh(d_{\mathrm{N}}/2\lambda_{\mathrm{N}})}{1+4\rho_{\mathrm{N}}\lambda_{\mathrm{N}}G_{\uparrow\downarrow}\coth(d_{\mathrm{N}}/\lambda_{\mathrm{N}})}.$$

Using the solutions of the coupled equations and the secular equation, the inverse spin-Hall voltage is calculated as

$$V = \frac{1}{4}\theta_{\mathrm{SH}}\frac{\hbar}{2e}\frac{L_V}{d_{\mathrm{N}}}g_m\frac{(\gamma_e h_x)^2}{\gamma_e H_s}\frac{(\gamma_n H_n)^4}{(\gamma_e H_a)^2}\left(\frac{H+H_D}{H_s}\right)^3\left[\frac{H_a H_s}{H(H+H_D)+H_a H_s}\right]^4\frac{1}{(\omega-\gamma_n H_p^*)^2+\Delta^2}.$$

At resonance $\omega = \gamma_n H_p^*$, the voltage is expressed in the form

$$V = V_0 \left(\frac{H + H_D}{H_s} \right)^3 \frac{\left[\frac{H_a H_s}{H(H + H_D) + H_a H_s} \right]^4}{\left(\left[\frac{H_a H_s}{H(H + H_D) + H_a H_s} \right]^2 + \frac{1}{\Delta_0 T_2} \right)^2},$$

where

$$V_0 = \theta_{\mathrm{SH}} \frac{L_V}{d_{\mathrm{N}}} \frac{g_m}{\alpha_M^2} \frac{\hbar \gamma_e h_x}{2e} \frac{h_x}{H_s}.$$

The absorbed radio-wave power $P_{\mathrm{abs}} = \langle h_x (\partial M_x / \partial t) \rangle$ is calculated as

$$P_{\mathrm{abs}} = \frac{1}{2} h_x^2 \frac{M_0}{H_a} \left(\frac{H + H_D}{H_s} \right)^2 \left[\frac{H_a H_s}{H(H + H_D) + H_a H_s} \right]^2 \frac{(\gamma_n H_n)^2 \Delta}{(\omega - \gamma_n H_p^*)^2 + \Delta^2}.$$

We assume $g_m \approx 1$ for $\rho_{\mathrm{N}} = 30\times10^{-6}$ Ωcm, $\lambda_{\mathrm{N}} = 1.5\times10^{-7}$ cm, $G_{\uparrow\downarrow} = 10^{12}\ \Omega^{-1}\mathrm{cm}^{-2}$ [S8], and $d_{\mathrm{N}} = 5$ nm. Using the values of $\theta_{\mathrm{SH}} = 0.08$, $\alpha_M = 0.0012$, $L_V = 0.3$ cm, $h_x = 5$ Oe, $H_{\mathrm{D}} = 4.6$ kOe, $H_s = 680$ kOe, we obtain $V_0 = 7.35$ mV. (When $\Delta_0 \propto (1/H_a) \propto T$ and $T_2 \propto T^{-1}$, $\Delta_0 T_2$ is independent of temperature.) The experimental data of H_a vs. T in the inset to Fig. 2**b** is well fitted by the relation: H_a [Oe] = 8.6/T [K] [S1], which is used to calculate the temperature dependence of V. Figure S1 shows the inverse spin Hall voltage as functions of the applied magnetic field H in (**a**) and of temperature T in (**b**), and the NMR linewidth as functions of H in (**c**) and of T in (**d**). The magnetic field dependence of V for $H_a = 5.5$ Oe and $T_2\Delta_0 = 200$ is plotted in Fig. 4**c**.

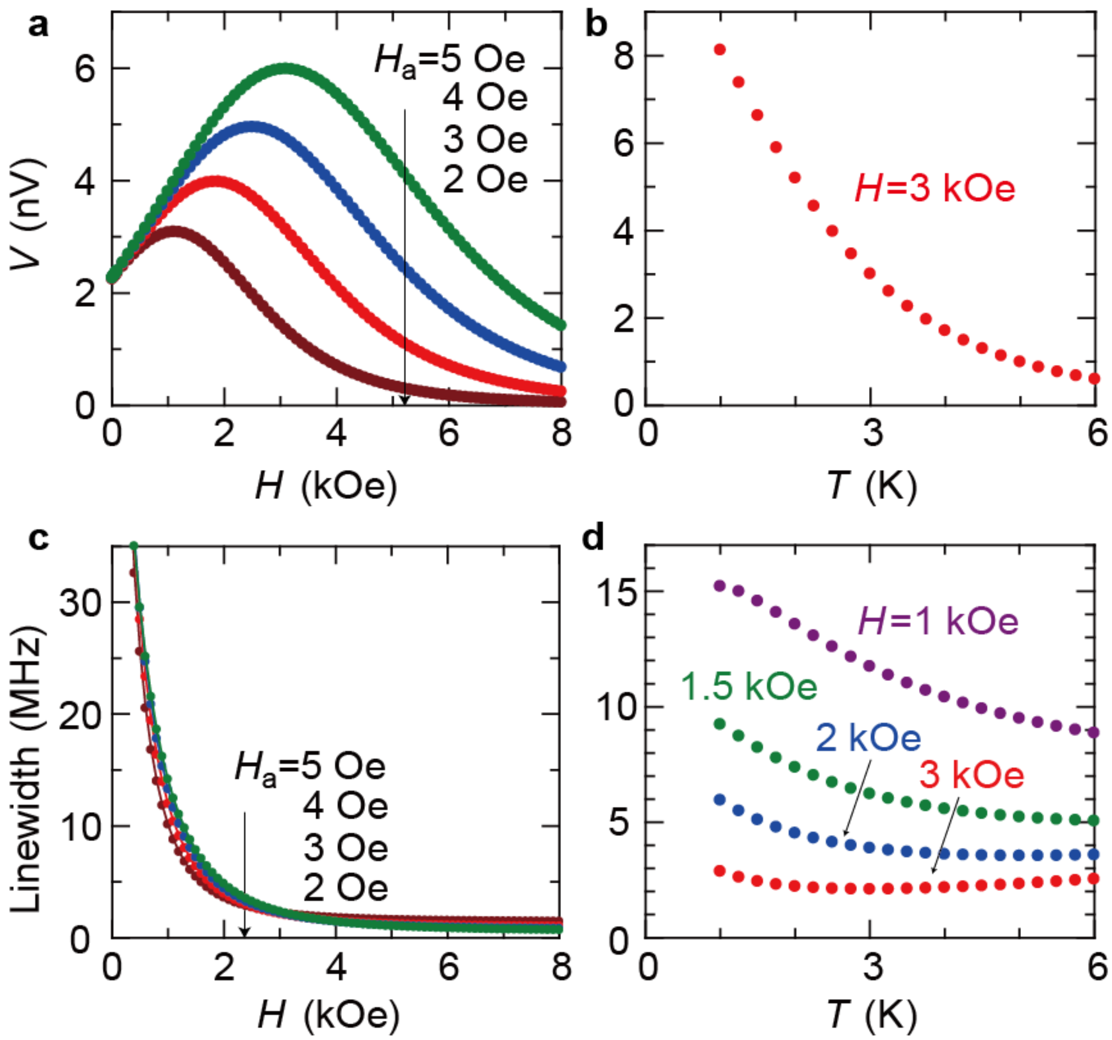

Figure S1: Calculated inverse spin Hall voltage and linewidth. (**a**), (**b**) Calculated inverse spin Hall voltage V as a function of (**a**) applied magnetic field (H) and (**b**) temperature (T). (**c**), (**d**) Calculated NMR linewidth Δ as a function of (**c**) H and (**d**) T.

References

[S1] Fink, H. & Shaltiel, D. Nuclear frequency pulling in a Dzyaloshinskii-Moriya-type weak ferromagnet: $MnCO_3$. *Phys. Rev.* **136**, A218 (1964).

[S2] Shaltiel, D. Nuclear magnetic resonance of $MnCO_3$ in the canted spin state. *Phys. Rev.* **142,** 300 (1966).

[S3] Tserkovnyak, Y., Brataas, A., Bauer, G. E. W. & Halperin, B. I. Nonlocal magnetization dynamics in ferromagnetic hybrid nanostructures. *Rev. Mod. Phys.* **87**, 1375 (2005).

[S4] Chiba, T., Bauer, G. E. W. & Takahashi S. Magnetization damping in noncollinear spin valves with antiferromagnetic interlayer couplings. *Phys. Rev. B* **92**, 054407 (2015).

[S5] Fink, H. & Shaltiel, D. High-frequency resonance of a weak ferromagnet: MnCO3. *Phys. Rev.* **130,** 627 (1963).

[S6] Heeger, A. J. & Teaney, D. T. Mn^{55} nuclear magnetic resonance in antiferromagnetic $RbMnF_3$. *J. Appl. Phys.* **35,** 846 (1964).

[S7] Borovik-Romanov, A. S., Bunkov, Yu M., Dumesh, B. S., Kurkin, M. I., Petrov, M. P. & Chekmarev, V. P. The spin echo in systems with a coupled electron-nuclear precession. *Sov. Phys. Usp.* **27**, 235-255 (1984).

[S8] Czeschka F. D., Dreher L., Brandt M. S., Weiler M., Althammer M., Imort I.-M., Reiss G., Thomas A., Schoch W., Limmer W., Hueb H., Gross R. & Goennenwein S. T. B. Scaling behavior of the spin pumping effect in ferromagnet-platinum bilayers. *Phys. Rev. Lett.* **107**, 046601 (2011).

(b) Spin Seebeck effect for Pt/$MnCO_3$

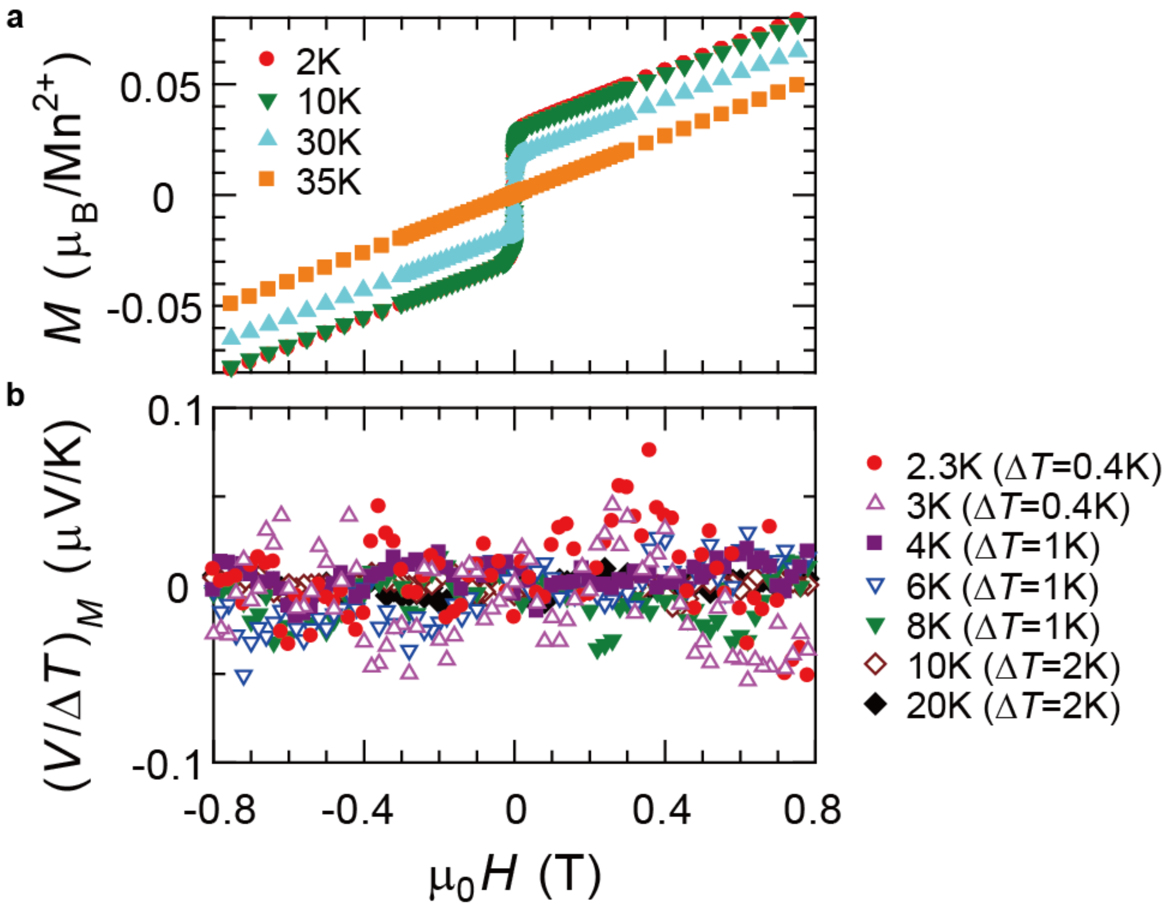

Figure S2: Spin Seebeck effect (SSE) in Pt/$MnCO_3$ below T_N of $MnCO_3$. (**a**),(**b**) Magnetic field (H) dependence of (**a**) magnetization (M) and (**b**) spin Seebeck voltage divided by the applied temperature difference ($V/\Delta T$) at selected temperatures. Here, H-linear (normal Nernst-type) signals are subtracted from the $V/\Delta T$ data. In the M-H curves, clear weak-ferromagnetic moments are observed below T_N (~35 K), whereas $V/\Delta T$ shows linear dependence on the magnetic field even at very low temperatures. This result shows that the very weak ferromagnetic moments (~ 0.03 μ_B/Mn^{2+}) due to the bulk Dzyaloshinskii-Moriya interaction in $MnCO_3$ only give rise to tiny spin Seebeck signals.

(c) Temperature dependence of radio-wave power loss in the spin-pumping measurement system

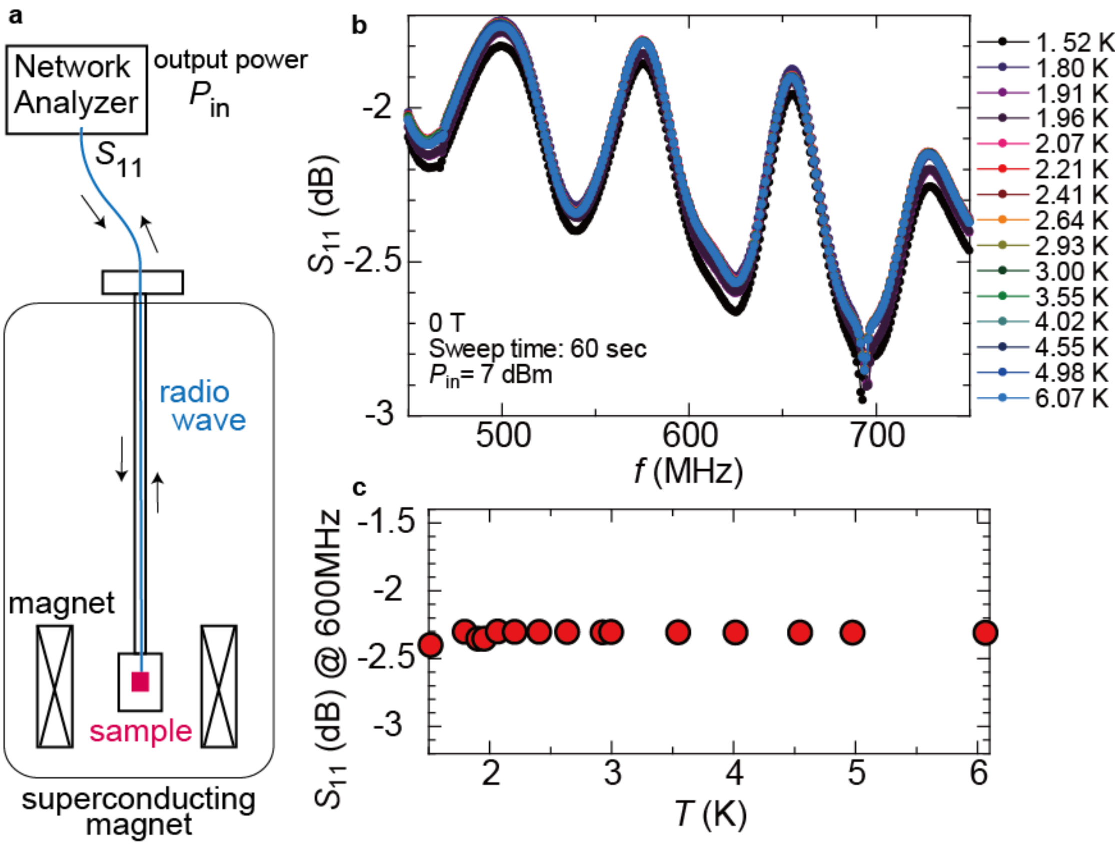

Figure S3: Radio-wave power losses in the spin pumping system at low temperatures. (**a**) Schematic illustration of the transmission path of the radio waves in the measurement system of spin pumping. Here, the power of a radio wave generated from a vector network analyzer is defined as P_{in}. The radio wave is transmitted through some connectors and cables, reaches the Pt/$MnCO_3$ sample, and then returns back to the vector network analyzer. The measured S-parameter S_{11} corresponds to the ratio of the returned radio-wave power (P_{ref}) to P_{in}. (**b**) Frequency dependence of S_{11} at various temperatures from 1.52 K to 6.07 K. The measurement was performed at zero magnetic field; NMR does not occur in this condition, and thereby only background signals originating from the measurement system are observed in the frequency spectrum. The background signals hardly change with temperature. (**c**) Temperature dependence of the S_{11} value at 600 MHz, the frequency where the NMR of $MnCO_3$ is observed (see the main text). The S_{11} value is almost constant. The background S_{11} value (≈ -2.3 dB) is taken into account (subtracted) in the estimation of the P_{abs} values in Fig. 3**c** in the main text.

(d) Sample characterization (AFM and X-ray diffraction data)

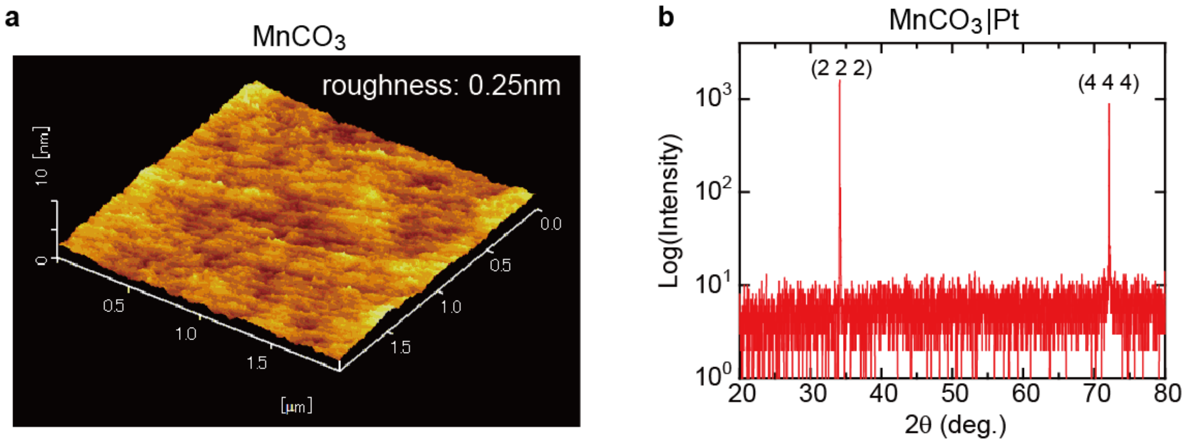

Figure S4: AFM and X-ray diffraction results. (a) Surface roughness of the $MnCO_3$ single crystal measured with an atomic force microscope (AFM). The averaged roughness is as small as 0.25 nm. (b) X-ray diffraction data for Pt/$MnCO_3$ used in the spin-pumping experiment. The peaks of (222) and (444) of $MnCO_3$ (in the rhombohedral setting) are observed, but no impurity peaks are discerned.

(e) Examination of interface magnetization using Hall-effect measurements for Pt/$MnCO_3$ at low temperatures

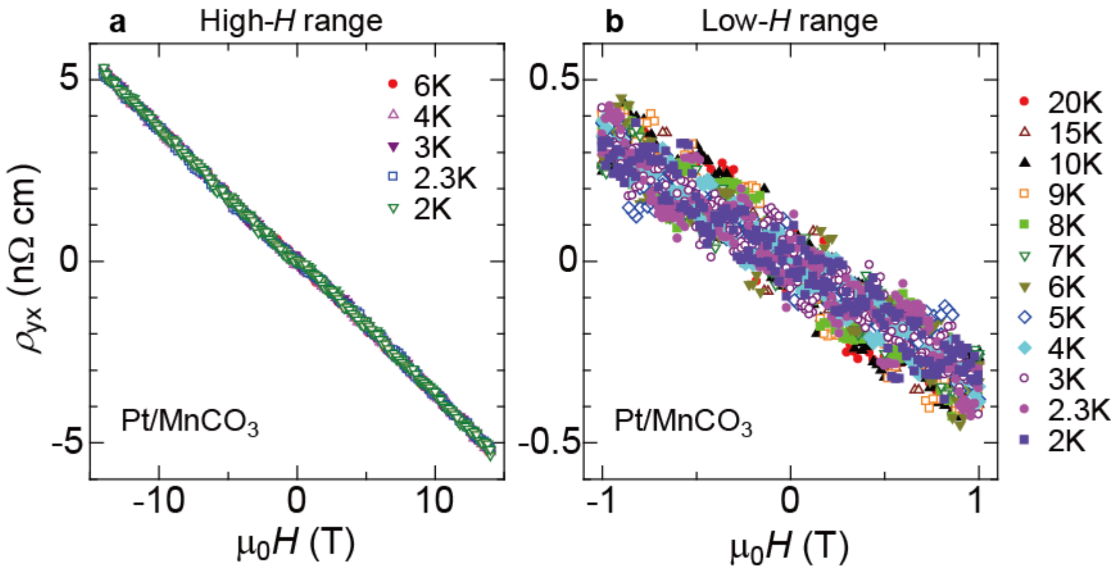

Figure S5: Hall effect in a Pt film grown on $MnCO_3$. Magnetic-field (*H*) dependence of Hall resistivity (ρ_{yx}) (**a**) in the high-*H* range up to 14 T and (**b**) in the low-*H* range up to 1 T. The Hall resistivity shows linear dependence on *H* even at low temperatures. The slopes (Hall coefficients) of *H*-ρ_{yx} curves remain constant in the entire temperature range from 2 K to 20 K.

(f) Input-power and sweep-direction dependence of NMR spin pumping

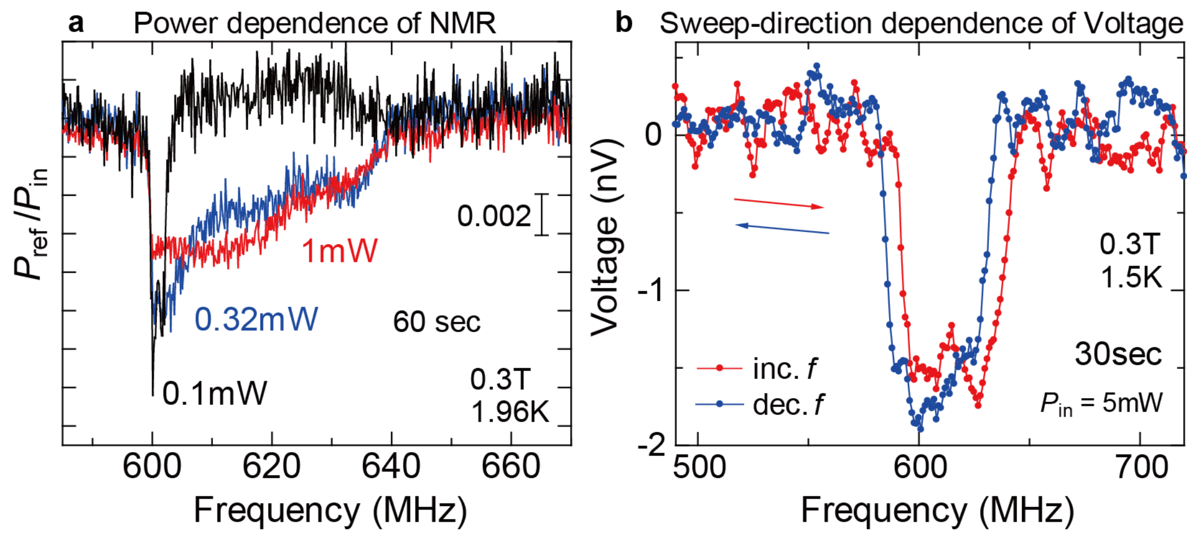

Figure S6: Input-power and sweep-direction dependence of NMR and voltage spectra for Pt/$MnCO_3$. (**a**) The input-power dependence of NMR spectrum is shown at the fixed sweep time of 60 s. Here, the frequency sweep was performed by increasing the frequency from 450 MHz to 750 MHz. When the input radio power is set at 0.1 mW, the linewidth is sharp, but it becomes broader with increasing input power levels. This power dependence is consistent with the scenario that the broadening of the NMR linewidth originates from a nonlinear effect of NMR reinforced by the nuclear-electron spin coupling. (**b**) Comparison of voltage spectra measured at 1.5 K and 0.3 T in increasing-frequency and decreasing-frequency scans. Here, the total time of the frequency sweep (between 450 MHz and 750 MHz) is set at 30 sec. Though the frequency range where the voltage signal is observed is shifted slightly by changing the sweep direction, the linewidths of the voltage signals are similar between these two scans. The similar linewidths independent of the frequency-scan directions rule out the possibility that the broadening of the NMR linewidth originates from increase in the sample temperature due to a heating effect; note that the NMR frequency becomes higher at higher temperatures (see Fig. 2**b** in the main text).

(g) Magnetic-field dependence of NMR spectra and spin-pumping voltages for Pt/MnCO₃

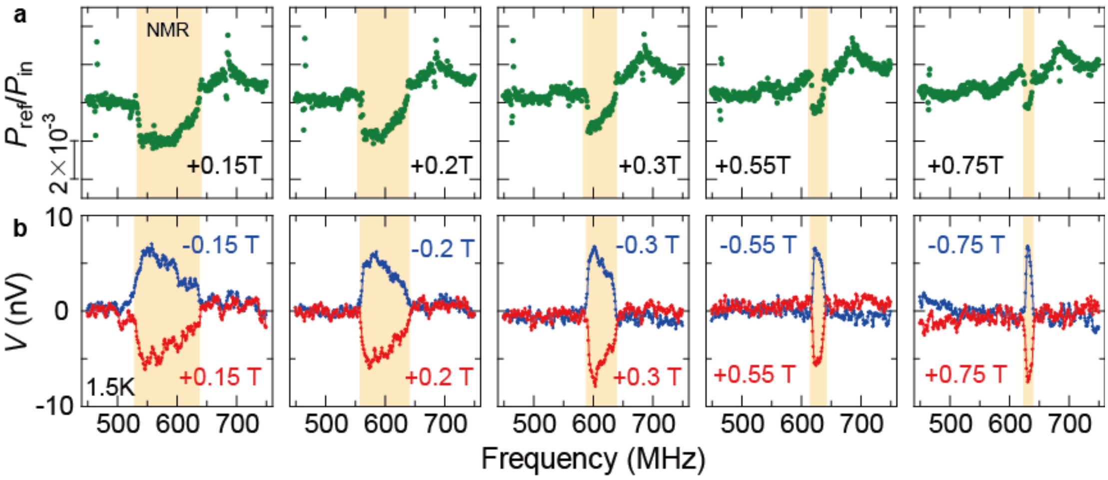

Figure S7: Magnetic field dependence of NMR spectra and spin-pumping voltages. (**a**) NMR absorption and (**b**) Voltage (V) spectra measured by applying various magnetic fields at 1.5 K, where the incident radio-wave power P_{in} is 5 mW. As the magnetic field increases, the linewidths of the NMR absorption spectra (**a**) and voltage peaks (**b**) decrease monotonically, as highlighted by the yellow shadow. The widths of the frequency ranges with the yellow shadow are defined as the "linewidths" of spectra, and are plotted in Fig. 4**c** in the main text.

(h) Data reproducibility for a different Pt/$MnCO_3$ sample

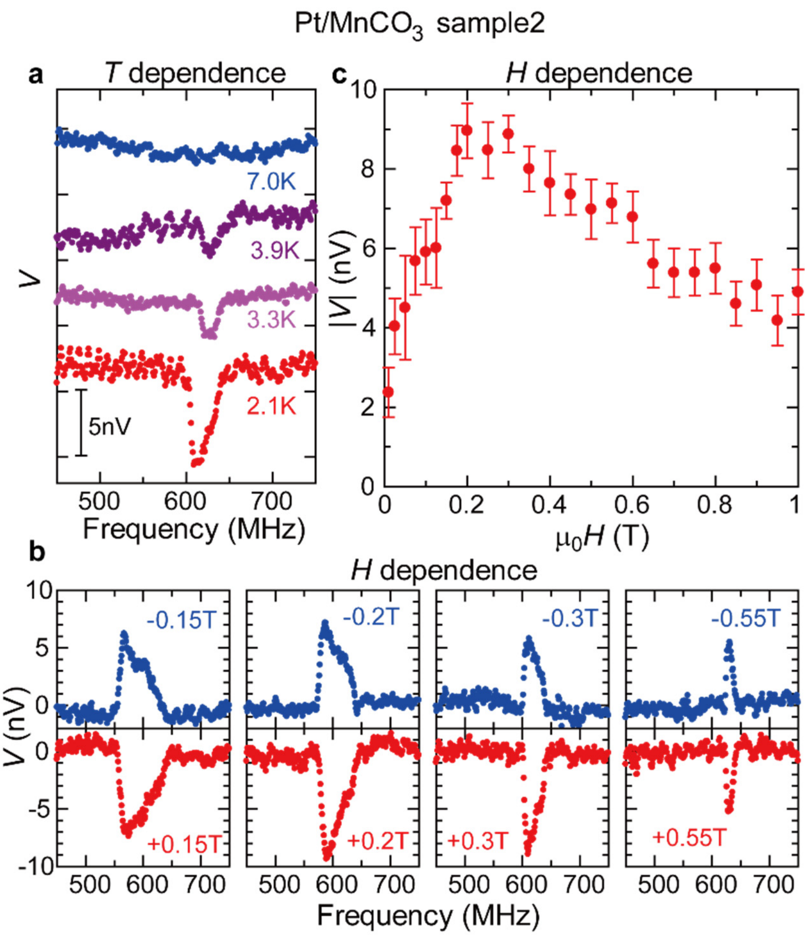

Figure S8: Temperature and magnetic-field dependence of spin-pumping voltages for a different Pt/$MnCO_3$ sample. (**a**) Voltage (V) spectra measured in the Pt layer around the NMR frequency of $MnCO_3$ at several temperatures, where the incident radio-wave power is 5 mW. The external magnetic field was fixed at +0.3 T. As temperature increases, the voltage peak height monotonically decreases, and the peak disappears at 7.0 K. This T dependence is consistent with that observed for the sample shown in the main text (see Fig. 2**d**). (**b**) Voltage (V) spectra measured by applying various magnetic fields (Hs) at 2 K, where the incident radio-wave power is 5 mW. As H increases, the linewidth of the voltage peak decreases monotonically, consistent with the result shown in Fig. S7. (**c**) Magnetic field (H) dependence of the voltage peak height. The data for positive magnetic fields in (**b**) is plotted here. With increasing H from zero, the voltage peak height first increases, and then starts to decrease at $\mu_0 H \sim 0.2$-0.3 T; this H dependence is in agreement with that shown in Fig. 4**a** in the main text.